UC Irvine
Faculty Publications

Title
Zonal flow vacillation and eddy forcing in a simple GCM of the atmosphere.

Permalink
https://escholarship.org/uc/item/76q8f0wr

Authors
Yu, J.-Y.
Hartmann, D. L.

Publication Date
1992-12-08

Copyright Information
This work is made available under the terms of a Creative Commons Attribution License, availalbe at https://creativecommons.org/licenses/by/4.0/

Peer reviewed

eScholarship.org Powered by the California Digital Library
University of California

Zonal Flow Vacillation and Eddy Forcing in a Simple GCM of the Atmosphere

JIN-YI YU AND DENNIS L. HARTMANN

Department of Atmospheric Sciences, University of Washington, Seattle, Washington

(Manuscript received 4 September 1992, in final form 8 December 1992)

ABSTRACT

Zonal flow vacillation with very long time scales is observed in a 3070-day simple GCM simulation with zonally symmetric forcing. The long lasting zonal wind anomalies suggest that zonal flow vacillation is self-maintained. Wave–mean flow interactions are investigated by composite analysis and transform Eulerian momentum budget analysis. Nonlinear life-cycle simulations are conducted to demonstrate that each extreme phase of the zonal flow vacillation is a quasi stable state and is self-maintained by the embedded synoptic eddies.

The first EOF mode of zonal-mean wind shows an out of phase relation between anomalies at 60°S and at 40°S with a barotropic structure. This structure is similar to the dominant vacillation pattern observed in the Southern Hemisphere. The composite jet stream in the high (low) index phase of zonal flow vacillation shifts poleward (equatorward) from the time-mean location and becomes broader (narrower) and weaker (stronger). Composite eddies in the high index phase tilt NW–SE and show mostly equatorward propagation, while eddies in the low index phase have "banana" shapes and propagate both equatorward and poleward. Transformed Eulerian momentum budget analyses show that the differences of wave propagation between two extreme phases result in the anomalous eddy forcing needed to maintain zonal wind anomalies against frictional damping.

Budget analyses also indicate that eddy momentum flux convergence is the major positive forcing in both the extreme and transition phases. Eddy baroclinic forcing exerts weak damping on the wind anomalies in the upper troposphere but acts together with residual circulation forcing to counteract frictional damping near the surface. The major balance during the index cycle is between eddy barotropic forcing and residual circulation forcing in the upper troposphere and between residual circulation forcing and frictional damping in the lower troposphere. Further comparisons of eddy forcing from various time-scale eddies show that the anomalous eddy forcing is primarily provided by synoptic time scales. Two nonlinear life-cycle simulations, started separately from the composite zonal flows of the two extreme phases and small-amplitude wavenumber 6 perturbations, display the intensification of initial wind anomalies by the growing eddies. A dual-jet stream structure appears in the life-cycle simulation started from the high index composite, and a more intense single jet stream structure evolves from the low index initial state.

It is noticed that maximum wind anomalies are established earlier at higher latitudes than at lower latitudes. This suggests that the mechanisms triggering transitions from one self-maintained phase to the other operate at higher latitudes. It is suspected that barotropic instability/stability is a possible triggering mechanism for transition from one state to another.

1. Introduction

Zonally symmetric variations have been observed both in the circulations of the Northern Hemisphere and the Southern Hemisphere. For instance, Lorenz (1951) found negative correlations between zonally averaged sea level pressures at 35°N and at 55°N, and Trenberth (1979) observed large interannual variability in the zonal-mean circulations of the Southern Hemisphere. The zonally symmetric variations are especially important in the Southern Hemisphere because of the relatively flat topography in this hemisphere. Karoly (1990) pointed out that the low-frequency variations of the Southern Hemispheric circulations are primarily zonally symmetric. The variations appear in two aspects of the hemispheric circulations. One is on the fluctuations of the westerly strength, and the other is on the meridional displacements of the jet stream location. Large amplitude fluctuations of the zonal kinetic energy have been observed by Webster and Keller (1975) in the upper troposphere. And Trenberth (1984), by comparing the circulation of the Global Weather Experiment (GWE) year to the mean circulations in 1972–80, found that the interannual variability in the GWE year was characterized by the meridional displacements of the main jet streams in the Southern Hemisphere.

Both the variations in zonal flow strength and jet stream location are qualitatively similar to the characteristic features in the zonal index cycle of Namias (1950). The zonal index was introduced by Rossby (1939) for the purpose of extended forecasting and was originally defined by the strength of westerlies between 35° and 55°N. It was later noticed by Willett (1948) that variations in the zonal flow strength were associated with latitudinal displacements of the jet stream

Corresponding author address: Dr. Jin-Yi Yu, Department of Atmospheric Sciences, AK-40, University of Washington, Seattle, WA 98195.

© 1993 American Meteorological Society

in the Northern Hemisphere. This vacillation phenomenon was referred as "the zonal index cycle" by Namias (1950). Because of the strong zonal symmetry in the circulations and more and better observations becoming available, the interest in the zonal index concept has been increasing for studies of Southern Hemisphere variability. Kidson (1988) applied EOF analysis to 15 years of 500-mb zonal mean winds to examine the dominant patterns of the zonal flow vacillations. A zonal index, based on the leading EOF mode, was then derived to characterize the variations of the Southern Hemisphere zonal circulation. The first EOF mode in his study has an out of phase relation between two centers of action at 40°S and at 60°S. Similar structure was seen in the rotated principal component analysis of 9 years of monthly mean zonal mean winds from European Centre for Medium-Range Weather Forecasts (ECMWF) and National Meteorological Center (NMC) analyses (Nigam 1990). Kidson (1988) and Nigam (1990) showed that this dominant mode had a barotropic structure.

Although the structures and time scales of the zonal flow vacillations in the Southern Hemisphere are now better known from observational analyses, the dynamics behind this phenomenon has not yet been completely understood. Trenberth (1984) argued that it was the anomalous convergence of eddy momentum that helped sustain the westerly anomalies against surface friction. Karoly (1990) examined the zonal circulations and transient eddy statistics in two extreme phases of the zonal vacillation in the Southern Hemisphere and found that the interaction between eddy fluxes and zonal flows helped maintain the wind anomalies. The importance of transient eddies was further discussed by Robinson (1991) in a two-layer GCM simulation. By analyzing the angular momentum budget projected onto his first rotated EOF structure, Robinson (1991) argued that the momentum fluxes from synoptic eddies sustained wind anomalies against friction, and the zonal index was driven by the small difference between the forcing of synoptic eddies and dissipation, together with forcing of low-frequency waves.

These studies suggest that the index cycle concept is useful for studying zonal flow vacillations, especially in the Southern Hemisphere. These studies also showed the importance of eddy forcing in supporting the zonal flow variations. More detailed studies on the relation between the zonal flow vacillation and the eddy forcing from observational analyses are difficult because of the lack of reliable eddy statistics in observations (Karoly 1990). Mechanistic studies, however, with simple GCMs are able to shed light on this relation. Though a two-layer simple GCM is enough for this kind of mechanistic study, a higher vertical-resolution GCM permits more detailed analysis of eddy fluxes and their interactions with the zonal flow. This paper will examine the variations of eddy structures and flux properties and their interaction with the zonal flows in different phases of the zonal flow vacillation. Emphasis will be placed on the relative contributions to the eddy forcing from eddy momentum fluxes and eddy heat fluxes. The time scale of the eddies that are most important to the zonal flow vacillation will also be investigated. The newly developed GCM and the simulation employed in this paper will be described in section 2. The zonal flow vacillations in the model simulation and the definition of the index cycle will be discussed in section 3. The associated zonal-mean circulations and eddy statistics will be presented in section 4, and the angular momentum budget during the index cycle will be analyzed in section 5. The relative importance of eddies with different time scales will be compared in section 6. Three baroclinic eddy life-cycle experiments are conducted in section 7 to illustrate the regime characteristics of the two extreme phases. A discussion on the possible reasons why the index cycle vacillates is presented in section 8.

2. Model description

The model employed in this study is a dry primitive equation model with global spherical geometry. The governing equations are primitive equations on σ coordinate (Phillips 1957). They are

$$\frac{\partial \xi}{\partial t} = -\nabla\cdot(\xi + f)\mathbf{V} - \mathbf{k}\cdot\nabla \times \left(RT\nabla q + \dot{\sigma}\frac{\partial \mathbf{V}}{\partial \sigma} - \mathbf{F}\right) - \nu\nabla^4\xi \quad (1)$$

$$\frac{\partial D}{\partial t} = \mathbf{k}\cdot\nabla\times(\xi + f)\mathbf{V} - \nabla\cdot\left(RT\nabla q + \dot{\sigma}\frac{\partial \mathbf{V}}{\partial \sigma} - \mathbf{F}\right) - \nabla^2\left(\Phi + \frac{\mathbf{V}\cdot\mathbf{V}}{2}\right) - \nu\nabla^4 D \quad (2)$$

$$\frac{\partial T}{\partial t} = -\nabla\cdot\mathbf{V}T + TD + \dot{\sigma}\gamma - \frac{RT}{C_p}\left(D + \frac{\partial \dot{\sigma}}{\partial \sigma}\right) + H_T - \nu\nabla^4 T \quad (3)$$

$$\frac{\partial q}{\partial t} = -D - \frac{\partial \dot{\sigma}}{\partial \sigma} - \mathbf{V}\cdot\nabla q \quad (4)$$

$$\sigma\frac{\partial \Phi}{\partial \sigma} = -RT, \quad (5)$$

where γ is the static stability and $\dot{\sigma}$ is the vertical motion on sigma coordinate. Here q is the logarithm of surface pressure, Φ is geopotential height, $\mathbf{F}$ represents the parameterization of frictional processes in the model, and H_T represents the diabatic forcing. The other symbols have conventional meanings.

This model is a full Galerkin model, which uses the spectral method for horizontal representation and the

finite-element method for vertical representation. The horizontal solution is triangularly truncated at total wavenumber 21 with spherical harmonics as the basic functions. Nonlinear terms in the governing equations are calculated by the transform technique of Eliasen et al. (1970) and Bourke (1972). The finite-element method uses linear interpolation functions as the basic functions, which are defined as follows:

$$e^i(\sigma) = \begin{cases} (\sigma - \sigma_{i-1})/(\sigma_i - \sigma_{i-1}), & \text{for } \sigma \in [\sigma_{i-1}, \sigma_i] \\ (\sigma_{i+1} - \sigma)/(\sigma_{i+1} - \sigma_i), & \text{for } \sigma \in [\sigma_i, \sigma_{i+1}] \\ 0, & \text{otherwise.} \end{cases} \tag{6}$$

The accuracy and stability of applying the finite-element method to a semi-implicit primitive equation model have been investigated by Béland et al. (1983) and Coté et al. (1983), respectively. A comparison of this method with the finite-difference method for the representation of vertical structure in a model atmosphere was discussed in Hartmann (1988). The vertical resolution of this model is variable and is chosen to be seven vertical levels (nodal points) in this study. The σ levels are placed at σ = 0.04, 0.20, 0.36, 0.52, 0.68, 0.84, and 1.00. The semi-implicit time scheme of Robert et al. (1972) is used for time differencing. This method allows a longer time step for integration, and a one-hour time step is chosen in this study. The derivation of governing equations and the application of the spectral transform method basically follow Daley et al. (1976). The applications of the finite-element method and the boundary conditions, $\dot{\sigma} = 0$ at $\sigma = 0.04$ and at $\sigma = 1.00$, are adapted from Béland and Beaudoin (1985).

This GCM includes the physical processes of frictional damping, radiative heating, dry convective adjustment, and biharmonic diffusion. The frictional damping in this model is parameterized by a quadratic friction $\mathbf{F} = -c(\sigma)|\mathbf{V}|\mathbf{V}$. The drag coefficient c is a function of altitude. It decreases linearly from $c = 10^{-6}$ s^{-1} at lower boundary to $c = 10^{-9}$ s^{-1} in the lowest interior node of the model atmosphere and increases again from the highest interior node to $c = 5 \times 10^{-8}$ s^{-1} at upper boundary. Radiation provides the only diabatic heating in the model and is parameterized by thermal relaxation of the Newtonian type. The heating is obtained by relaxing temperature T back to a prescribed equilibrium temperature T^* with a relaxation time τ. That is, $H_T = (T^* - T)/\tau$, where $T^* = T_0(\sigma) + \Delta T \cos 2\phi$ and $\tau = 15$ days. Here T_0 is the global-mean temperature, and $2\Delta T$ is the equator to pole temperature difference; ΔT is set to 30 K in most σ levels, 0 K in the second upper level, and -15 K in the top level. Dry convective adjustment of Manabe et al. (1965) is adopted to prevent the model from becoming statically unstable. Biharmonic diffusion is applied in the vorticity, divergence, and thermodynamic equations. These terms are used to simulate the dissipation effect from the subgrid scales. The diffusive coefficient ν is set to 6×10^{-16} m^4 s^{-1}, which gives a 1.5-day damping time on total wavenumber 21. Several tests have been conducted with this model to verify the model dynamics. The normal mode calculation of Simmons and Hoskins (1977) and the life cycle calculation of Simmons and Hoskins (1978) were repeated with this model and similar results were obtained.

In the simulation conducted here, a Gaussian-shaped mountain is placed in the northern model hemisphere and flat topography in the southern model hemisphere. It is designed for the purpose of future comparison between mountain and no-mountain hemispheres. The Gaussian-shaped mountain is 4 km high with e-folding widths of 20° in longitude and 15° in latitude. The analyses presented here are from the no-mountain Southern Hemisphere of this simulation. The mountain in the northern model hemisphere has little effect on the Southern Hemisphere simulation described here. The model is spun up from rest for 300 days. The end of this integration is used as the initial condition for another 3070 days of integration. Data are sampled daily on sigma surfaces and are linearly interpolated to pressure surfaces on 100, 200, 300, 500, 700, 850, and 1000 mb.

3. Zonal flow vacillation and index cycle

During the 3070 days of simulation, the jet stream vacillates meridionally between high and middle latitudes. Along with this vacillation, the maximum wind speed also varies with time. The zonally averaged westerly winds on day 83 and on day 495 are shown in Fig. 1 as an example of this vacillation. On day 83, there is a narrow jet stream located at 40°S, and its maximum wind speed is much more than 40 m s^{-1}, which is the maximum wind speed of the time-mean jet stream. In clear contrast to day 83, there are two jet streams on day 495; one at 30°S and the other at 52°S. The wind speeds of both jet streams are smaller than the time-mean jet stream. Vacillations occur not only in the upper-level jet streams but also in the surface westerlies. The surface westerlies shrink to middle latitudes on day 83 but expand to high latitudes on day 495.

The power spectrum of the 300-mb zonally averaged westerlies at 41°S (not shown) increases as the frequency decreases, but no spectral peak passes the 99% a priori significance level. This suggests that the zonal flow vacillation in the simulation is a low-frequency phenomenon with no preferred period, that is, red noise. EOF analysis is applied to the covariance matrix of the zonally averaged winds to examine the spatial pattern of the vacillation. The structure of the first EOF mode (referred as the EOF-1 mode, hereafter), which explains more than 67% of the variance, is shown in

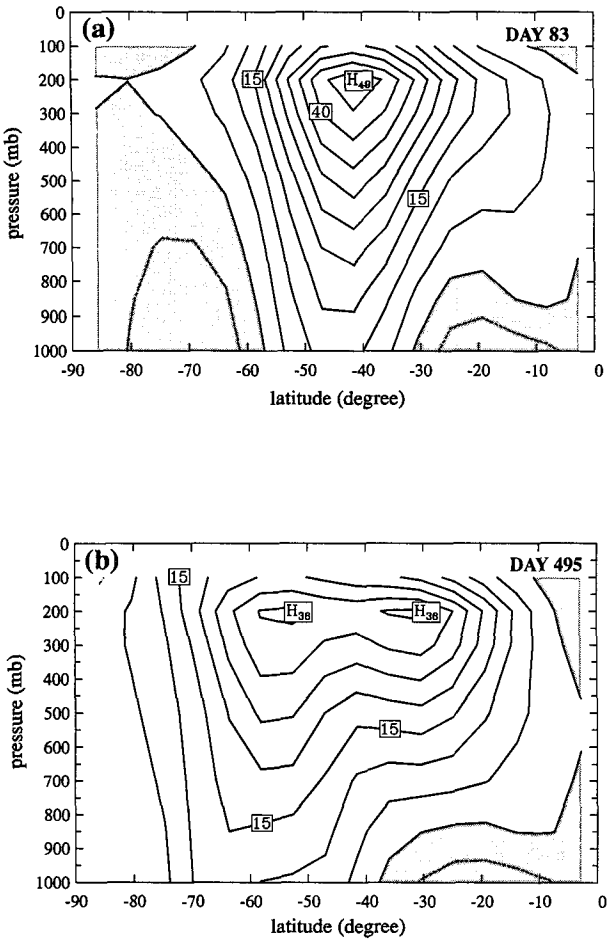

FIG. 1. Zonally averaged zonal winds on (a) day 83 and (b) day 495. Easterlies are contoured by dashed lines and are shaded.

Fig. 2. This mode shows that the wind anomalies centered at 40°S are out of phase with the wind anomalies centered at 60°S and at 25°S. The amplitudes are larger at 60°S and at 40°S than at 25°S. It also shows that the zonal flow vacillation has a barotropic structure with the maximum amplitudes at 300 mb. Both the meridional and vertical structures of the EOF-1 mode in this simulation are similar to the dominant vacillation patterns observed in the Southern Hemisphere by Kidson (1988) and Nigam (1990).

Since the principal component of the EOF-1 mode represents the amplitude and phase of the EOF-1 mode, its temporal variation indicates how the zonal flow vacillates. Figure 3 displays the time series of the principal component of the EOF-1 mode, and it shows that the principal component oscillates intermittently between positive values and negative values. This figure also shows that the time series may remain in either extreme positive values or extreme negative values for long periods of time, on the order of 100 ~ 200 days, before shifting to the other extreme. A bimodal behavior, however, is not supported by the histogram of the principal component. Based on these characteristics, an index cycle is used to qualitatively describe the zonal flow vacillation. An index cycle consists of two extreme phases and two transition phases. The two extreme phases are the high index phase and the low index phase. In Rossby's (1939) original introduction, the "high" zonal index and "low" zonal index were referred to the westerly strength averaged in midlatitudes. It has been pointed out by Namias (1950) that the maximum wind displaces toward lower latitudes in the low index phase, and the maximum wind speed in this phase is actually stronger than that in the high index phase. We will maintain Rossby's definition of high and low index so that the "high" index and the "low" index refer to the latitudinal locations of the jet stream and not maximum wind speed. With this convention, the high (low) index phase is referred to the situation when the jet stream is located at a latitude higher (lower) than the time-mean location. The sign of EOF-1 is defined such that the positive phase of the EOF-1 mode is the high index phase, and the negative phase of the EOF-1 mode is the low index phase. One of the transition phases is the transition from the low index phase to the high index phase. During this process, the principle component increases from a negative value to a positive value. So this phase is referred to as the "positive transition phase" for the sake of discussion. Similarly the "negative transition phase" refers to the shifting from the high index phase to the low index phase in the index cycle.

The composite method will be used to examine the zonal-mean circulations and eddy properties in each phase of the index cycle. The selection of data for composition is based on the principal component of the EOF-1 mode. Those days that have principal components among the top (bottom) 15% are averaged to-

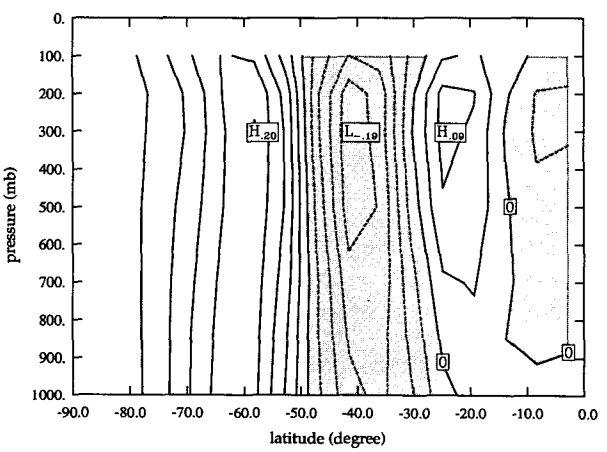

FIG. 2. Meridional–vertical structure of the first EOF mode of the zonally averaged zonal wind anomalies in 3070 days of simulation. The negative values are shaded and the contour interval is 0.04.

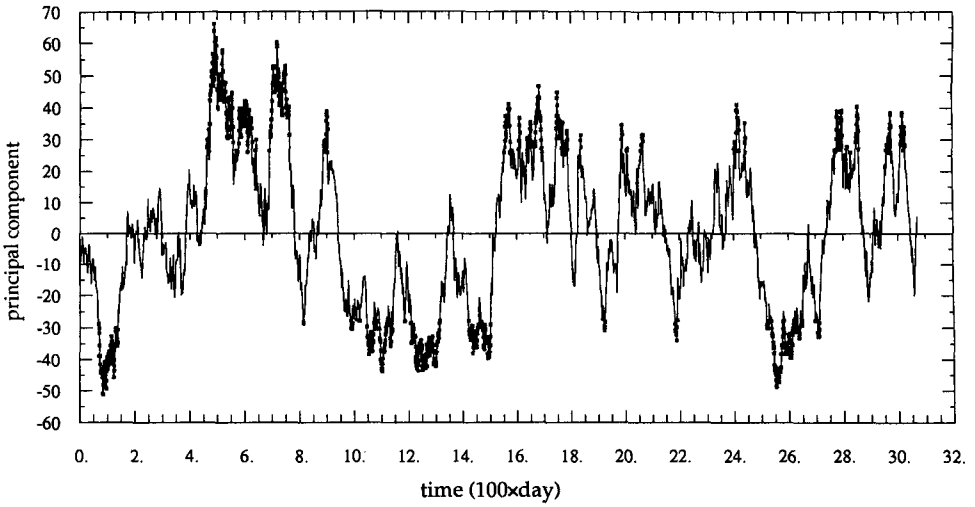

FIG. 3. Principal components of the first EOF mode. The square points indicate the days selected for composition in the high index phase (positive side) and in the low index phase (negative side). There are 460 points on each side.

gether to form the high (low) index phase composite. The days selected by this criterion are marked by square points in Fig. 3. It shows that the data are well sampled through the major peaks of the time series. During the transition phases, it is the time tendency of the principal component rather than the principal component itself that matters. So the selection criterion is based on the time tendency of the principal component. Moreover, since the zonal flow vacillation is a low-frequency phenomenon, time tendencies are calculated from the 50-day low-pass filtered principal components. The response function of this filter is shown in Fig. 4, along with two other filters that will be used later. Those days that have time tendencies among the top (bottom) 15% of positive (negative) values are selected for composition in the positive (negative) transition phase. In order to avoid overlap between sampling the transition phases and the extreme phases, data already used in the extreme phases are excluded from the transition phases. There are 460 days of data in each phase of the index cycle.

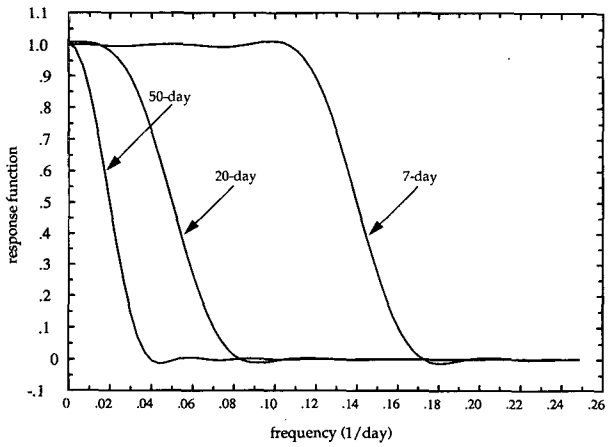

FIG. 4. Response functions of the 50-day, 20-day, and 7-day low-passed filters.

4. Zonal circulations and eddy properties

The composite zonally averaged zonal winds in the extreme phases are shown in Fig. 5. In the high index phase there is a broad and weak jet stream at 48°S on 200 mb. This is about 5° ~ 10° poleward from the time-mean location. Accompanying the poleward shift of the jet stream, surface westerlies extend to higher latitudes and span between 38°S and 72°S. In contrast to this, the composite zonal flow in the low index phase has a strong and narrow jet stream near 40°S at 200 mb, and the surface westerlies are confined between 30°S and 60°S. The difference between these two composites (not shown) has an anomaly structure similar to the EOF-1 mode, and its maximum amplitude is about 12 m s^{-1}. This is close to the magnitude of zonal flow vacillation observed in the Southern Hemisphere (Nigam 1990; Karoly 1990).

When the composite jet stream displaces equatorward in the low index phase, the polar cell of the mean meridional circulation (not shown) expands into 60°S. The polar cell is much weaker in the high index phase than in the low index phase. The composite temperatures (not shown) exhibit meridional displacements of the thermal gradient in thermal wind balance with the zonal wind vacillations. The temperature difference between the extreme phases is similar to that associated with the observed zonal vacillation in the Southern

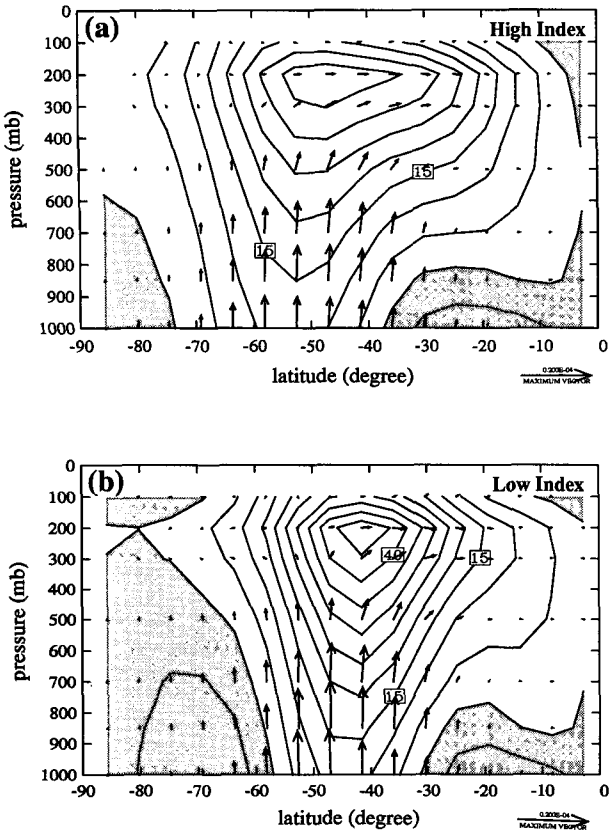

FIG. 5. Composite zonal-mean zonal winds and EP flux vectors in (a) the high index phase and (b) the low-index phase. EP flux is defined as $(-\cos\phi[u'v'], f\cos\phi\{[v'\theta']/[\theta]_p\})$. The contour interval for composite zonal winds is 5 m s^{-1}. Easterlies are shaded.

Hemisphere (Karoly 1990). The composite zonal winds, meridional winds, and temperatures in the positive transition phase are similar to those in the negative transition phase, and these composites are very close to the time-mean averages (not shown). It will be shown later that the eddy properties are different between the two transition phases, even though the zonal mean winds are similar, and that these differences are consistent with the opposite accelerations of wind anomalies in two transition phases.

How the eddies respond to the variations in the zonal flow is examined by first investigating the eddy structures in the index cycle. This is done by the averaged one-point correlation method. To take advantage of the zonal symmetry in this model hemisphere, the one-point correlation maps are calculated with a base point moving along a base latitude. Each correlation map is then rotated to have the base point located at 180°E. An averaged one-point correlation map is obtained by averaging all rotated correlation maps together. The averaged one-point correlation maps of the 300-mb relative vorticity are shown in Fig. 6. The base-point latitude is 41°S in this figure. The eddies in the high index phase have strong northwest to southeast tilts, while the eddies in the low index phase have banana-shaped structures. The difference between eddy structures indicates that the wave propagation and momentum fluxes in the two extreme phases are different. Also seen in Fig. 6 are the different orientations of the correlation maxima between two extreme phases. The correlation maxima in the high index phase run from higher latitudes to lower latitudes, but the coefficient maxima in the low index phase line up between 30°S and 50°S. This difference suggests that eddies in the high index phase propagate out of the jet stream toward the equator, while the eddies in the low index phase are confined to propagate along the jet stream. The waveguide feature in the low index phase is caused by the strong and narrow jet stream in that phase. The eddy structures between two transition phases are also different, but the differences are not as big as those between two extreme phases (not shown). This less obvious difference becomes apparent in the eddy momentum fluxes that will be shown later. Generally speaking, the eddy structure in the transition phases is a mixture of the structures in the high and low index phases.

The eddy kinetic energy in the low index phase is stronger than that in the high index phase (Fig. 7a). This is consistent with the fact, as can be seen in Fig.

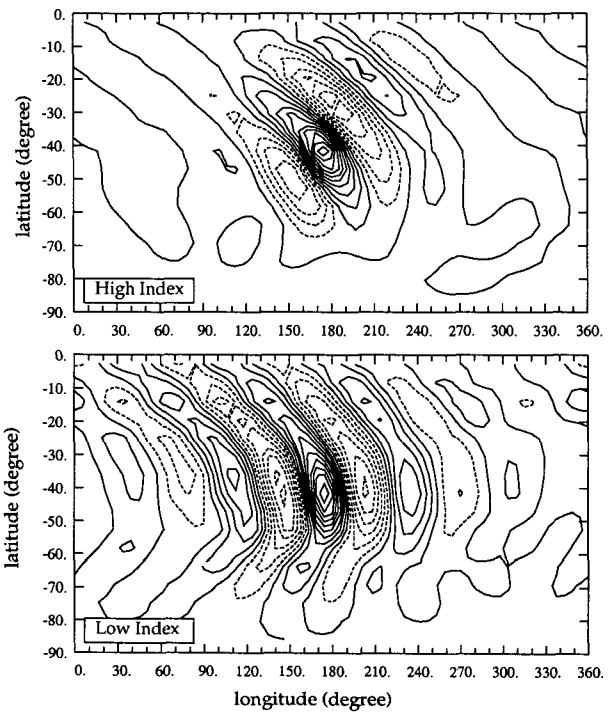

FIG. 6. Averaged one-point correlation maps of 300-mb relative vorticity in (a) the high index phase and (b) the low index phase. The method of obtaining the averaged one-point correlation maps is explained in the text. The base latitude is 41.5°S. The contour interval is 0.1.

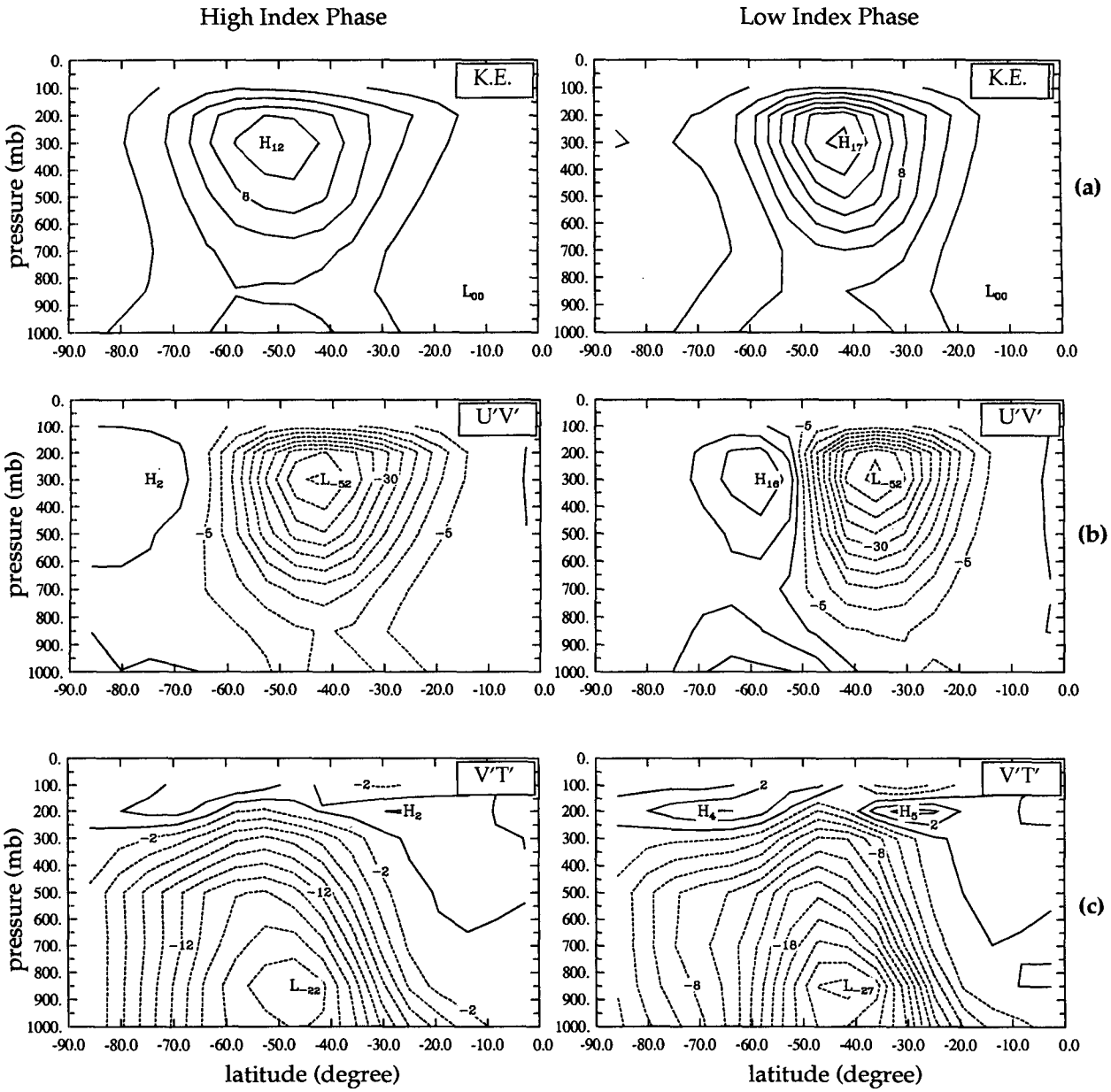

FIG. 7. Composite eddy statistics in the high index phase (left panels) and in the low index phase (right panels): (a) eddy kinetic energy, (b) eddy momentum flux, and (c) eddy heat flux. Contour intervals are 20 $m^2 s^{-2}$ for eddy kinetic energy, 5 $m^2 s^{-2}$ for eddy momentum flux, and 2 K m s^{-1} for eddy heat flux.

5, that the vertical wind shear in the low index phase is stronger than in the high index phase. The composite eddy momentum fluxes (Fig. 7b) reflect the structural differences between the eddies in the high and in the low index phases. The eddy momentum fluxes in the high index phase are mostly poleward, but there are both poleward and significant equatorward eddy momentum fluxes in the low index phase. The equatorward fluxes at higher latitudes in the low index phase are related to the southwest to northeast tilt of the banana-shaped eddy structure. The heat fluxes at most latitudes are poleward in both extreme phases and have their maxima in the lower troposphere (Fig. 7c). The eddy heat flux maximum in the low index phase is confined to a narrower area than the maximum in the high index phase. Also the eddy heat flux maximum is stronger in the low index phase and is shifted to lower latitudes, consistent with the change in the latitude of the jet stream.

The composite eddy statistics suggest that variations in the zonal flows cause different developments and propagations of eddies in the index cycle. The corre-

sponding variations between zonal flows and eddy activities are better seen by superimposing EP-flux vectors onto the composite zonal-mean winds (Fig. 5). Because of the broader jet stream and the larger area of surface westerlies, the eddies in the high index phase develop in a broad latitudinal area between 30°S and 75°S and propagate equatorward after reaching the middle to upper troposphere. In the low index phase, eddy development is confined to the narrow surface westerly zone, and the eddies propagate both poleward and equatorward in the upper troposphere. So the large amplitude EP-flux vectors in the low index phase are more concentrated in the middle latitudes.

The composite eddy kinetic energy and eddy momentum fluxes at 300 mb and eddy heat fluxes at 850 mb in four phases of the index cycle are shown in Fig. 8. These figures are used to illustrate how eddy properties vary during the two transition phases. When the model atmosphere shifts from the low index phase toward the high index phase (i.e., the positive transition phase), the kinetic energy maximum decreases and moves to higher latitudes (Fig. 8a). In the negative transition phase, the energy maximum increases from the minimum value in the high index phase and shifts toward midlatitudes. This shows that the storm track moves along with the upper-level jet stream during the index cycle. This phenomenon has also been observed by Karoly (1990) in the Southern Hemisphere. Variations similar to those in the eddy kinetic energy are also seen in the eddy momentum flux (Fig. 8b) and in the eddy heat fluxes (Fig. 8c). Unlike eddy kinetic energy or eddy heat flux, whose maximum and minimum values are found always in the extreme phases, eddy poleward momentum flux has its maximum value in the negative transition phase. More importantly, the differences between the two transition phases are more significant in eddy momentum fluxes than in eddy kinetic energies or eddy heat fluxes. This suggests that the eddy momentum flux is the process that dominates the transition phases. The significance of the differences between four different phases is supported by the similar results (not shown) obtained from another 3070-day simulation where a 1-km mountain is placed in the northern model hemisphere.

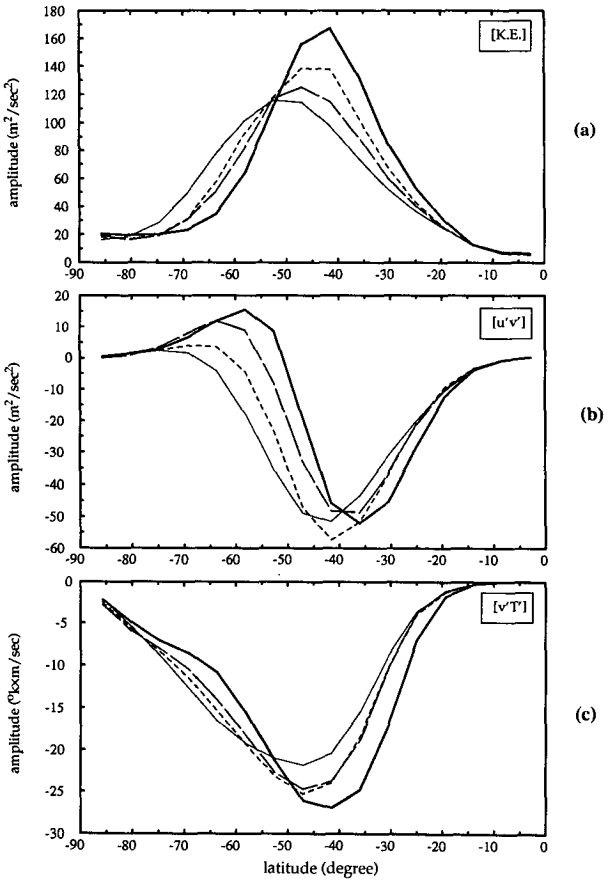

FIG. 8. Composite eddy statistics in four phases of the index cycle. Panel (a) is for eddy kinetic energy at 300 mb, (b) is for eddy momentum flux at 300 mb, and (c) is for eddy heat flux at 850 mb. Curves with thin lines are for the high index phase, thick lines for the low index phase, short-dash lines for the positive transition phase, and long-dash lines for the negative transition phase.

5. Zonal angular momentum budget

It has been mentioned in section 3 that the large-amplitude wind anomalies in the extreme phases are able to last for long periods of time. With the presence of strong friction at the surface, those wind anomalies have to be maintained by some forcing. In the transition phases, forcing is also required to accelerate wind anomalies from one phase of the EOF-1 mode to the other. Forcing through eddy–zonal flow interaction is the likely mechanism. There are two ways in which eddies can interact with zonal flows: one is through the convergence of eddy momentum fluxes and the other through the convergence of eddy heat fluxes. In addition, we must consider the important influence of the mean meridional circulation. In order to analyze both parts of eddy forcing explicitly, the transformed Eulerian angular momentum equation, similar to the one discussed in Edmon et al. (1980), is used. This momentum budget is expressed as

$$\frac{\partial [u]}{\partial t}\cos\phi = f[v^*]\cos\phi + \frac{1}{a\cos\phi}\frac{\partial}{\partial\phi}(-[u'v']\cos^2\phi) + \frac{\partial}{\partial p}\left(f\frac{[v'\theta']}{[\theta]_p}\cos\phi\right) + F_x\cos\phi, \quad (7)$$

where $[(\ )]$ is the zonal average of a quantity $(\ )$, v^* is the residual meridional velocity, defined as

$$[v^*] = [v] - \frac{\partial}{\partial p}\left(\frac{[v'\theta']}{[\theta]}\right), \quad (8)$$

and F_x is the longitudinal component of the frictional damping. The term

$$\frac{1}{a\cos\phi}\frac{\partial}{\partial\phi}(-[u'v']\cos^2\phi)$$

related to eddy momentum fluxes is referred to as the barotropic part of eddy forcing, and the term

$$\frac{\partial}{\partial p}\left(f\frac{[v'\theta']}{[\theta]_p}\cos\phi\right)$$

related to eddy heat flux is referred to as the baroclinic part of the eddy forcing. In order to understand how wind anomalies are maintained in the extreme phases, the angular momentum budget in the low index phase is subtracted from the angular momentum budget in the high index phase. Similarly, the momentum budget in the negative transition phase is subtracted from that in the positive transition phase to investigate how the wind anomalies in the transition phases are accelerated. The resulting angular momentum budgets are interpreted as the balance between the time tendency of the wind anomalies of the EOF-1 mode and the barotropic part and baroclinic part of the anomalous eddy forcing, Coriolis forcing on anomalous residual circulation, and friction on the zonal flow anomalies. Here "anomalous" refers to the deviations from the time-mean average, that is, the part associated with the index cycle.

The barotropic part and the baroclinic part of the anomalous eddy forcing in the extreme phases are shown in Fig. 9a and Fig. 9b. The barotropic part is largest in the middle to upper troposphere. The forcing accelerates westerly anomalies at both high and low latitudes but decelerate anomalies at middle latitudes. This forcing pattern is in phase with the positive EOF-1 mode and thus helps to maintain the zonal flow anomalies in the extreme phases. The baroclinic part of the anomalous eddy forcing is largest in the lower troposphere. It exerts weak damping on the EOF-1 mode in the upper troposphere but tends to help maintain wind anomalies near the surface. The major momentum balance in the upper troposphere is between the anomalous eddy barotropic forcing and the Coriolis forcing by the anomalous residual circulation. This can be seen in Fig. 9c, where the net advective forcing:

$$f[v^*]\cos\phi+\frac{1}{a\cos\phi}\frac{\partial}{\partial\phi}(-[u'v']\cos^2\phi)+\frac{\partial}{\partial p}\left(f\frac{[v'\theta']}{[\theta]_p}\cos\phi\right)$$

is shown. The net advective forcing is largest at the surface where it counteracts anomalous friction and is basically in phase with the positive phase of the EOF-1 mode. Mass integration of the net advective forcing from 1000 mb to 800 mb is about the same magnitude as the mass integration of the eddy barotropic forcing between 600 mb and 100 mb. So the barotropic part

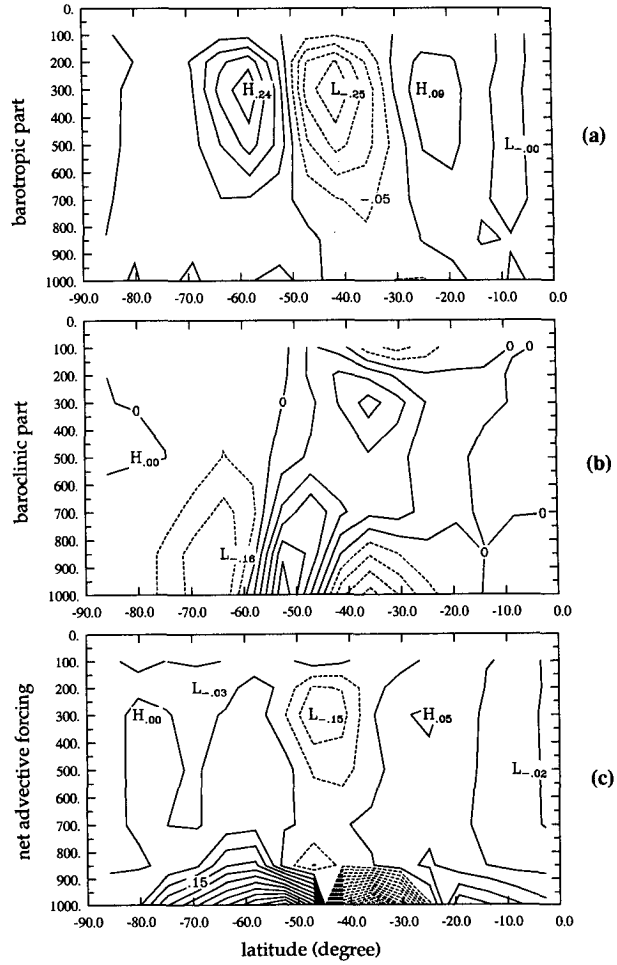

FIG. 9. Forcing differences between two extreme phases. The differences (i.e., the anomalous part) are obtained by subtracting forcing terms of Eq. (7) in the low index phase from those terms in the high index phase. Panel (a) is the barotropic part of the anomalous eddy forcing and panel (b) is the baroclinic part of the anomalous eddy forcing. Panel (c) is the net advective forcing. Contour intervals are 5×10^{-6} m s^{-2}, and contour labels are given in units of 10^{-4} m s^{-2}.

of the anomalous eddy forcing in the upper troposphere is transferred down to the surface by the anomalous residual circulation, where it counteracts surface friction. It should be pointed out that there is still significant residual in the total forcing, though the actual momentum tendency is small. The problem of large residuals in transformed Eulerian momentum budgets, even when applied to model output, has been noticed in Randel (1990). Including the other primitive equation terms, which are neglected here, does not resolve this problem. As will be shown later, the residual is quite small in the transition phase difference where the eddy heat flux difference is small. It is suspected that numerical errors associated with interpolation to pressure coordinates, especially in the calculations related to vertical derivatives of eddy heat flux, are the main

sources for the large residuals in the momentum budget. Nevertheless, the tendencies are determined by the dominant terms discussed above, and the differences between the composites should give the correct impression about the cause of the tendency.

Both parts of the anomalous eddy forcing in the transition phases are shown in Figs. 10a and 10b. It should be noted that a smaller contour interval, compared to that used in Fig. 9, is used in these figures because of the smaller difference between the two transition phases. The barotropic part has a forcing pattern similar to the eddy barotropic forcing in the extreme phases, so it helps to establish the wind anomalies during the transition phase. The baroclinic part is relatively weak compared to the barotropic part, and it does not show a clear forcing or damping effect on the EOF-1 mode. The total forcing from the anomalous eddy forcing, anomalous frictional damping, and anomalous Coriolis forcing during the transitions is shown in Fig. 10c. It shows that the total forcing accelerates the westerly anomalies at high and low latitudes and decelerates the wind anomalies between 30°S and 50°S, and it has a barotropic structure with the maximum amplitudes in the upper troposphere. The net forcing structure is very similar in structure to the zonal wind tendency. The importance of the barotropic part of the anomalous eddy forcing demonstrated here is consistent with the eddy property analysis in section 4, where it is shown that the major difference between two transition phases is their eddy momentum fluxes.

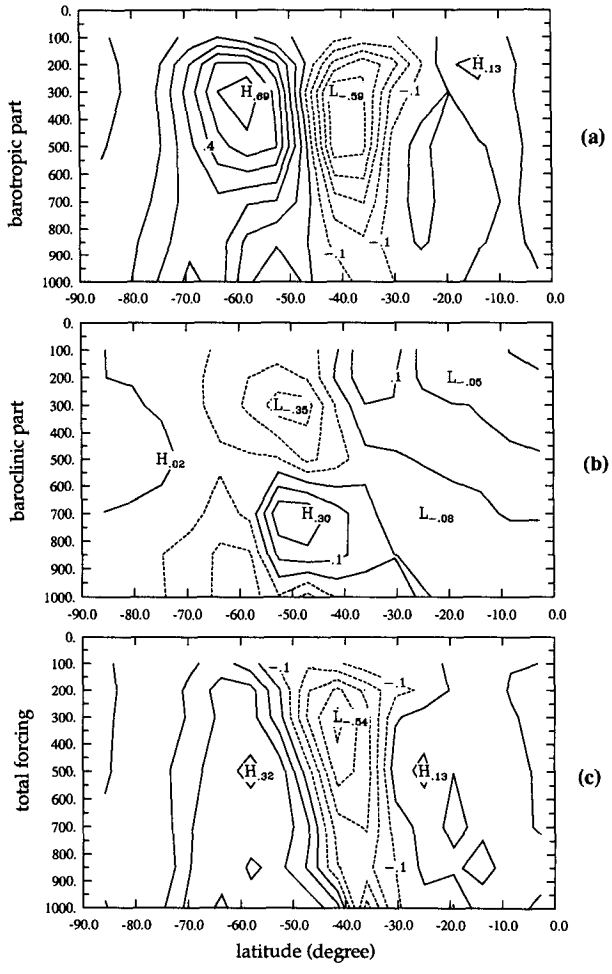

FIG. 10. Forcing differences between two transition phases. The differences are obtained by subtracting forcing terms of Eq. (7) in the negative transition phase from those terms in the positive transition phase. Panel (a) is the barotropic part and panel (b) is the baroclinic part of the anomalous eddy forcing. Panel (c) is the total forcing difference. Contour intervals are 1×10^{-6} m s^{-2}, and contour labels are given in units of 10^{-4} m s^{-2}.

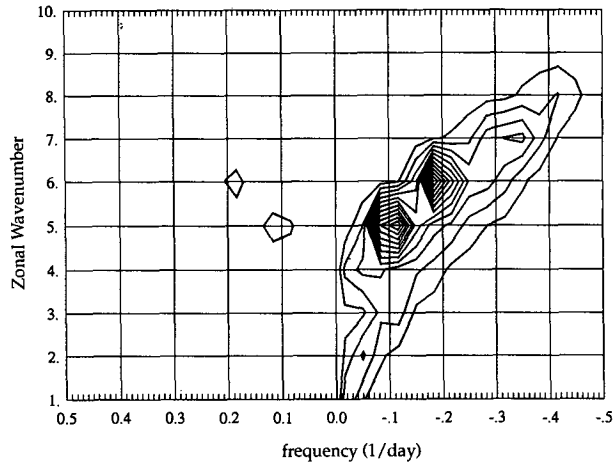

FIG. 11. Space–time spectrum of relative vorticity at 41.5°S on 300 mb. The spectra are averaged every 50 frequency bands before being contoured. Contour interval is 2×10^{-14} s^{-2}.

6. Forcing from high- and low-frequency eddies

From the angular momentum analyses, it has been shown that anomalous eddy forcing, especially the barotropic part, is important to the zonal flow variations. It is necessary to know what time scales of eddies provide most of this forcing. Space–time spectral analysis is applied to the 300-mb eddy relative vorticity at 41°S, and the frequency band–averaged spectrum is shown in Fig. 11. This figure shows that there are two dominant space and time scales in eddy spectra. One has a longer time scale near 10 days and a zonal scale of wavenumber 5, and the other has synoptic time scale around 5 ~ 6 days and a zonal scale of zonal wavenumber 6. Two time filters are used to filter eddies into the high-frequency and low-frequency components. One is a 20-day low-pass filter, which separates the eddies with both synoptic time scale and 10-day time scale from the rest of the eddies. The other is a 7-day low-pass filter, which separates the synoptic time-scale eddies from the 10-day time-scale eddies. Their response functions are shown in Fig. 5.

Comparisons between unfiltered eddies, 20-day low-pass filtered eddies, and 20-day high-pass filtered eddies (not shown) show that eddies with time scale longer than 20 days have little contribution to the total eddy kinetic energies, eddy momentum fluxes, and eddy heat fluxes. A similar comparison between unfiltered eddies, 7-day low-pass filtered eddies, and high-pass filtered eddies is shown in Fig. 12. The eddy kinetic energies and eddy momentum fluxes at 300 mb and the eddy heat fluxes at 850 mb, calculated from these three groups of eddies, are shown in Figs. 12a–c. Since it is known that 20-day low-pass filtered eddies have little contribution to the total eddy energy and fluxes, 7-day low-pass filtered eddies are primarily dominated by eddies with time scale between 7 and 20 days, especially the ~10 day eddies. Figure 12 shows that both 7-day low-pass filtered eddies and high-pass filtered eddies have comparable contributions to the total eddy kinetic energy and momentum fluxes, while the contributions

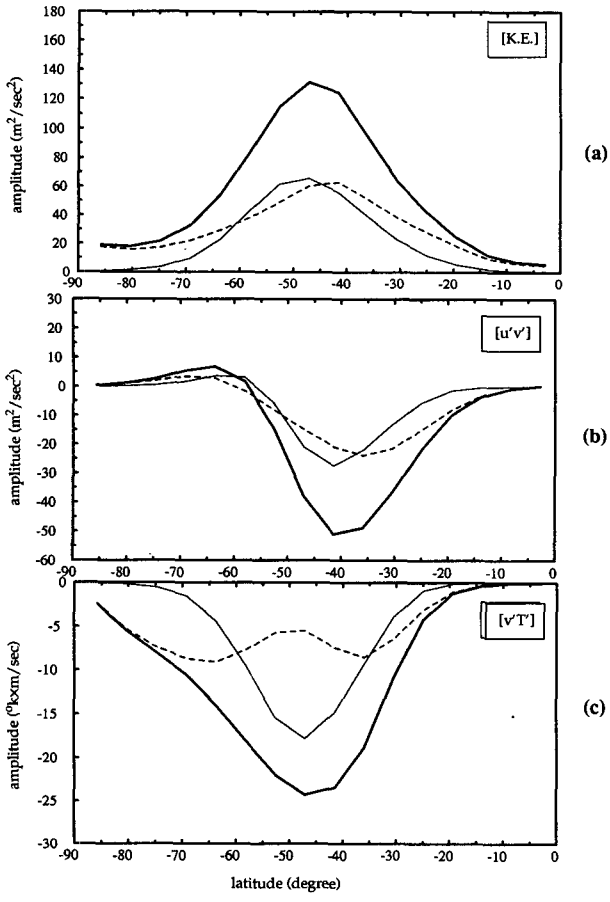

FIG. 12. Time-mean eddy statistics from unfiltered eddies, 7-day low-pass filtered eddies, and 7-day high-pass filtered eddies. Panel (a) is the eddy kinetic energy, panel (b) is the eddy momentum flux, and panel (c) is the eddy heat flux. Curves with thick lines are calculated from the unfiltered eddies, curves with thin lines are calculated from the 7-day high-pass filtered eddies, and curves with short dash lines are calculated from 7-day low-pass filtered eddies.

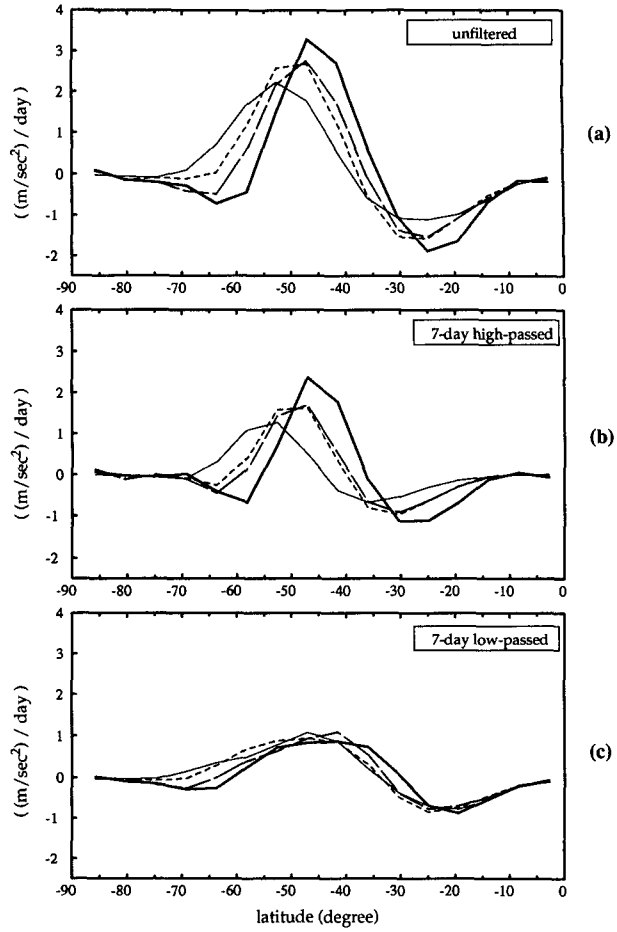

FIG. 13. Barotropic part of the 300-mb anomalous eddy forcing in four phases of the index cycle. Panel (a) is calculated from unfiltered eddies, (b) from 7-day high-pass filtered eddies, and (c) from 7-day low-pass filtered eddies. Curves with thin lines are for the high index phase, thick lines for the low index phase, short-dash lines for the positive transition phase, and long-dash lines for the negative transition phase.

to total eddy heat fluxes are dominated by high-pass filtered eddies in midlatitudes and by low-pass filtered eddies in higher and lower latitudes at the edges of the jet stream. It has been shown, however, in the momentum budget analysis that it is the anomalous eddy forcing (i.e., the varying part of the eddy forcing), that supports the zonal flow vacillations. The barotropic parts of eddy forcing in four phases of the index cycle are compared in Fig. 13. As expected, the eddy barotropic forcing from the unfiltered eddies has large variations during the index cycle. In the low index phase, eddy barotropic forcing accelerates westerlies between 35°S and 55°S and decelerates winds elsewhere. The latitudinal profile of this forcing is similar to the distribution of the surface westerlies, and this forcing maintains a narrow and strong jet stream at 40°S in the low index phase. When the atmosphere shifts from

the low-index phase to the high index phase, that is, the positive transition phase, the forcing pattern moves to higher latitudes and decreases its strength. The strength of eddy barotropic forcing reaches its minimum in the high index phase when the westerlies between 40°S and 70°S are accelerated and are elsewhere decelerated. In the negative transition phase, the forcing pattern shifts back to middle latitudes and increases its amplitude. The eddy barotropic forcing from the 7-day high-pass filtered eddies displays a similar kind of variation in the index cycle, but the forcing from 7-day low-pass filtered eddies experiences little variation during the cycle (Fig. 13c). The comparisons in Fig. 13 indicate that eddies with synoptic time scale provide most of the anomalous eddy forcing to support the zonal flow variations, especially in the extreme phases. This result is consistent with the Robinson (1992) study in which he argues that momentum fluxes from synoptic eddies sustain wind anomalies in his two-layer GCM simulation.

7. Nonlinear life-cycle experiments

To demonstrate the importance of the eddy forcing in maintaining the zonal flow anomalies in the extreme phases and the regime characteristics of the two extreme phases, three 50-day baroclinic eddy life-cycle experiments are conducted. The first experiment (experiment H) uses the composite zonal winds from the high index phase as the initial condition, the second experiment (experiment L) uses the composite winds from the low index phase, and the third experiment (experiment M) use the time-mean average. A small zonal wavenumber 6 perturbation is added to each zonally symmetric initial state in the beginning of simulations. The same damping and radiative forcing are applied in these experiments. The time–latitude cross sections of zonal mean winds from experiment H and experiment L are shown in Fig. 14. In the simulation using the composite wind from the high index phase (experiment H), the broad jet structure in the initial condition is reinforced by the eddy as it goes through nonlinear life cycles during the simulation. A dual-jet stream feature, which is often observed in the high index phase, appears after day 20. In the simulation using the composite wind from the low index phase (experiment L), the growing eddy intensifies the narrowness of the jet stream.

The eddy structures in experiment H and experiment L, examined by the averaged one-point correlation maps (not shown), have the same wavenumber 6 dominance but different tilts. In experiment H, eddies have northwest to southeast tilt as seen in the high-index phase, while the eddies in experiment L have a banana-shaped structure as seen in the low index phase.

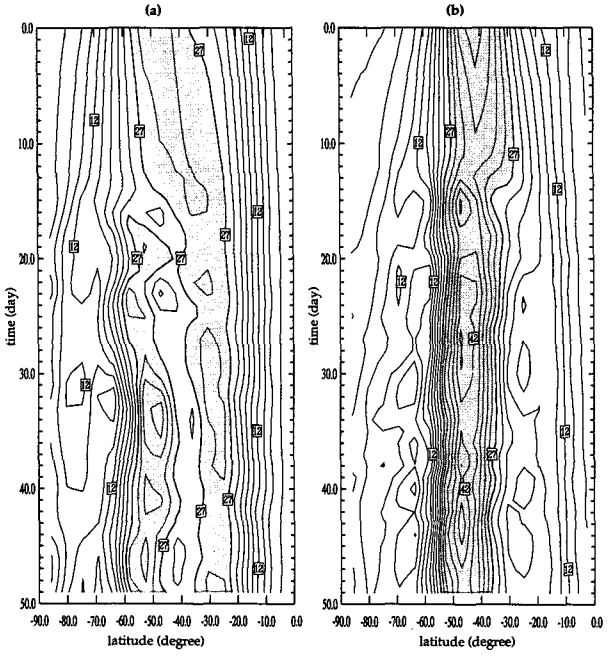

FIG. 14. Time–latitude cross sections of zonally averaged zonal winds during two nonlinear life-cycle experiments. Panel (a) is for an initial condition of the high index phase zonal wind composite and panel (b) is from an initial condition of the low index composite. Both simulations are perturbed with zonal wavenumber 6 of small amplitude. Contour intervals are 3 m s^{-1}. Wind speeds greater than 27 m s^{-1} are shaded.

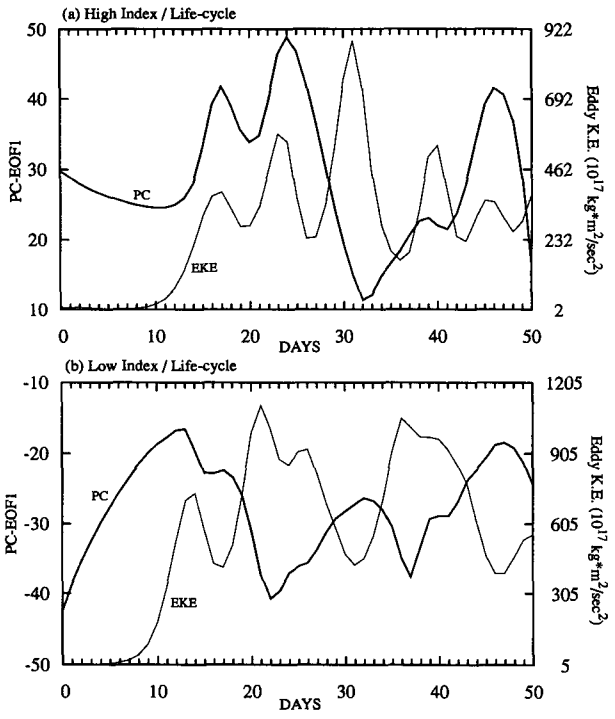

FIG. 15. Temporal evolution of the principal component of the EOF-1 mode and the hemispherically and vertically integrated eddy kinetic energy during the life-cycle experiments. Panel (a) shows the life cycle in the simulation started from the high-index composite and (b) is the life cycle from the low-index composite. Thick lines represent principal components (PC), and thin lines represent eddy kinetic energy (EKE).

Further examination on the time evolutions of the principal components of the EOF-1 mode and the eddy kinetic energy (Fig. 15) reveals more interesting facts in these two life-cycle experiments. In both experiments, the principal components are pushed toward the extreme values in experiments H and L after the eddy energy reaches maximum. This is not the case in the first few days of Experiment L when eddy adjusts to the normal-mode structure and during the third life cycle of the experiment H when the eddy kinetic energy is exceptionally high. The principal component appears to reach a local extreme value about 1 day after the eddy kinetic energy is maximum, which is consistent with the fact that eddy momentum flux usually reaches a maximum 1 day after the eddy kinetic energy in the life cycle of baroclinic waves. This supports the results from momentum budget analyses that eddy barotropic forcing is the main forcing to the maintenance of zonal flow vacillation. Experiment H and experiment L strongly suggest that both the high index phase and the low index phase are self-maintained through the baroclinic eddy–zonal flow interaction.

Experiment M is designed to further test if other initial states can be maintained as in experiment H and experiment L. During the 50-day simulation, the time-mean averaged wind structure in the initial condition of experiment M evolves into a dual-jet structure (not shown) similar to the one seen in experiment H. Experiment M suggests that the time-mean average wind structure is not a natural extremum as in the cases of experiment H and experiment L. This result supports the suggestion that the low index phase and the high index phase are the quasi-stable states in the model atmosphere. The result from experiment M seems to suggest that the high index phase is the preferred state of the model atmosphere. The number of occurrences of the low index phase (1550 days), however, is similar to that of the high index phase (1520 days) during the 3070 days of simulation and so does not show a preference for the high index phase. A carefully designed series of life-cycle experiments started from different zonal index values may be helpful in understanding the mechanism of transition within the index cycle.

8. Discussion

The maintenance of the zonal flow anomalies in the extreme phases and the acceleration of wind anomalies in the transition phases have been shown to be primarily provided by anomalous eddy forcing, especially the barotropic part of it. But it has not yet been shown why the atmosphere is triggered to leave the self-maintained low or high index phases and shift to the other self-maintained phase. We have noticed, in time–latitude cross sections of the zonal flow anomalies, that maximum wind anomalies appear in high latitudes a few days earlier than in middle and lower latitudes. The first 1000 days of this cross section is shown in Fig. 16, along with the principal components of the EOF-1 mode. Both wind anomalies and principal components are 50 day low-pass filtered. This figure shows that the negative wind anomalies near day 90 reach their maximum values at 60°S about 10 days earlier than the maximum is reached at 40°S and about 20 days earlier than at 25°S. Similar time-lag relations are also observed near day 490 and day 720 in this figure, though the time lags are different. These time shifts appear quite clearly in time-lag correlations computed from the entire 3070-day integration. In order to place more weight on the latitudes with large wind anomalies, the time lag–latitude cross section of the covariance, rather than the correlation, between wind anomalies at 58.1°S and other latitudes is shown in Fig. 17. It shows that, on average, large wind anomalies are established at 40°S about 3 days later than those at 60°S. It is about another 10 days later that anomalies are established at 25°S.

If there is any mechanism, other than chaos, that controls the initial shifting of the index cycle, the above time-lag phenomenon suggests that this mechanism might operate at higher latitudes. The $\beta - [\bar{u}]_{yy}$ calculated from the time-mean zonal wind $[\bar{u}]$ (not shown) changes signs at the polar flank of the time-mean jet stream. This suggests that barotropic instability might be a possible mechanism to trigger or facilitate the model atmosphere shifting out of one self-maintained extreme phase toward the other. Examination of the meridional gradient of the potential vorticity, however, does not show a sign change in any phase of the index cycle. Although poleward flank of the jet stream is always near neutral stability, further examination of barotropic instability in the model simulation, such as the calculation of growth rate and structure of the most unstable mode, will be necessary to examine this possible triggering mechanism.

9. Conclusions

A very low frequency vacillation in the zonally averaged zonal wind in the model hemisphere with zonally symmetric forcing is found in a 3070-day simulation. This vacillation consists of variations of zonal-mean westerlies at high, middle, and low latitudes. EOF analysis indicates that the dominant spatial pattern has a barotropic structure and two major centers of action at 40°S and 60°S with opposite phases. The time series of principal components of this dominant EOF mode indicates that the model atmosphere vacillates between the positive and negative phases of the EOF-1 pattern and is able to stay in either phase for long periods of time before shifting to the other phase. An index cycle is derived to describe the characteristics of this vacillation. Each cycle consists of four phases: the high index phase, the negative transition phase, the low-index phase, and the positive transition phase. The properties

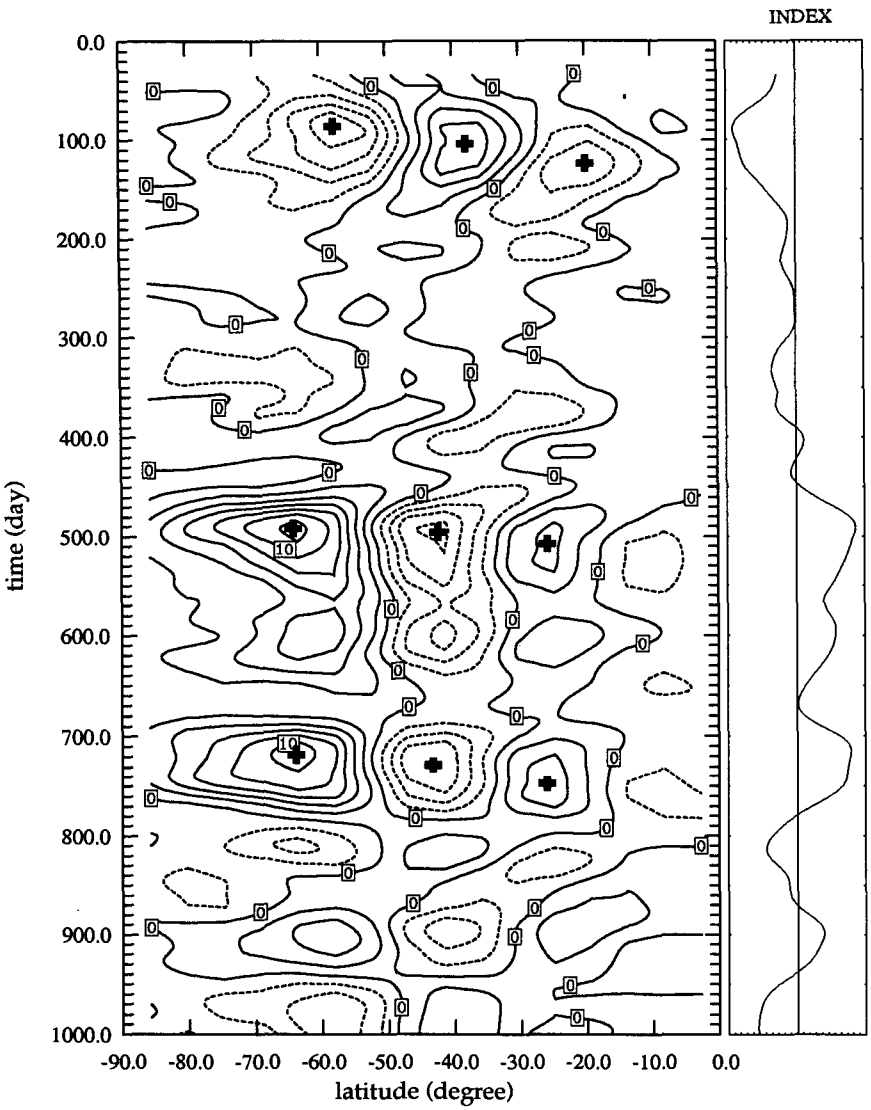

FIG. 16. Time–latitude cross section of zonal-mean westerly anomalies in the first 1000 days of the simulation. The principal components of the EOF-1 mode in the first 1000 days are also shown on the right panel. The zonal-mean wind anomalies and the principal components are 50 day low-pass filtered. The centers of local extreme anomalies are marked by plus signs. Contour interval for wind anomalies is 2 m s^{-1}.

of the zonal circulations and the eddies in each phase are studied with the composite method. The transformed Eulerian angular momentum equation is applied with these composited statistics to investigate how the index cycle is maintained. Emphasis is placed on the roles of eddy–zonal flow interaction through eddy momentum flux and heat flux convergences.

In the extreme phases of the index cycle, eddy structures and eddy flux properties differ as a result of the differences in the zonal flow. The generation of eddies in the lower troposphere is confined to a small latitudinal area in the low index phase because of the narrow jet stream and surface westerlies. The autocorrelation patterns of these eddies have a banana-shape structure that produces both poleward and equatorward momentum fluxes at the flanks of the jet stream. Because of the broad jet and area of surface westerlies, the eddies in the high index phase develop within a broad area in the lower troposphere and propagate equatorward in the upper troposphere over most latitudes. The corresponding changes in eddy properties feed back on wind anomalies through the convergence of eddy momentum flux and eddy heat flux. Transformed Eulerian angular momentum budget analyses show that the eddies produce different forcing in different phases of the index cycle, and this anomalous eddy forcing supports

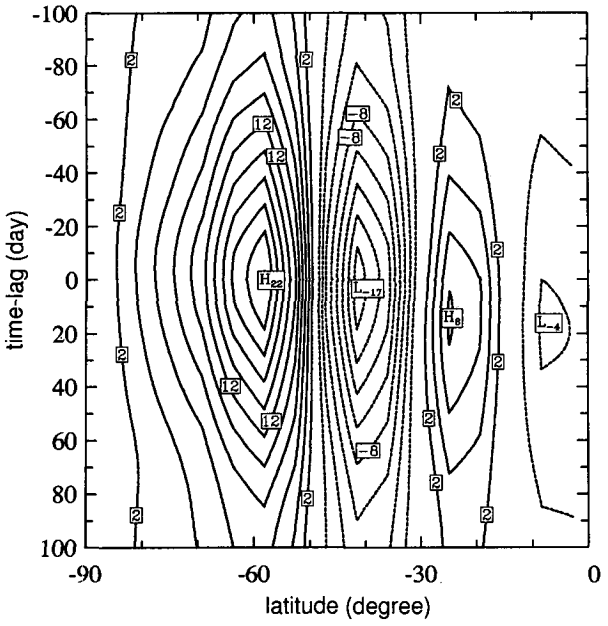

FIG. 17. Time lag–latitude cross section of the covariance of 50-day low-passed zonal-mean wind on 300 mb. The base latitude is 58.1°S. The contour interval is 2 $m^2 s^{-2}$.

the wind anomalies during the index cycle. The barotropic part of the anomalous eddy forcing helps maintain the wind anomalies in the extreme phases and generates the wind anomalies in the transition phases. The baroclinic part of anomalous eddy forcing damps wind anomalies in the upper troposphere but helps maintain the lower-tropospheric anomalies in the extreme phases. The influence of eddy baroclinic forcing is weak in the transition phases. The major terms in the zonal momentum balance during the index cycle are eddy barotropic forcing and Coriolis forcing by the residual circulation in the upper troposphere and the residual circulation forcing and frictional damping in the lower troposphere. Although eddies with both ~10-day time scales and synoptic time scales have comparable contributions to the eddy kinetic energies, eddy momentum fluxes, and eddy heat fluxes, most of the anomalous eddy forcing that drives the index cycle is from eddies with time scales less than 7 days. Therefore, the synoptic time scale eddies are the most important eddies for supporting zonal flow vacillations in the model.

Two experiments using the composite zonal winds of the high-index phase and the low index phase as the initial conditions are perturbed by small amplitude wavenumber 6 eddies and are integrated for 50 days. The narrowness of the jet stream in the experiment using the low index phase composite winds is intensified by the growing eddies, while a dual-jet stream feature appears in the experiment using the high index composite winds. These two experiments demonstrate that the baroclinic eddy–zonal flow interaction is able to maintain wind anomalies in the extreme phases. A third experiment using the time-mean zonally averaged winds as the initial condition evolves into a dual-jet stream structure similar to the experiment using the high index composite winds. The result of the third experiment and the first two experiments suggests that both the high-index phase and the low index phase are self-maintained quasi-stable states of the model atmosphere.

It is noticed that maximum wind anomalies are established earlier at higher latitudes than at middle latitudes during the index cycle. This suggests that the mechanism, if there is one, that triggers the model atmosphere to shift from one extreme phase to the other may operate at higher latitudes. Barotropic instability associated with the strong meridional shear at the polar flank of the jet stream is suspected to be one such possible mechanism. Although the necessary condition for barotropic instability is not satisfied for the composite zonal-mean states, more investigation on the barotropic instability associated with the model atmosphere may provide understanding on the role of barotropic instability in the zonal flow vacillation.

Acknowledgments. We thank Dr. W. A. Robinson and Dr. D. J. Karoly for their helpful comments and suggestions. This research was supported by the Climate Dynamics Program, Atmospheric Sciences Division of the National Science Foundation under Grant ATM 90-06123. Computational support was supplied by the San Diego Supercomputer Center.

REFERENCES

Béland, M., and C. Beaudoin, 1985: A global spectral model with a finite-element formulation for the vertical discretization: Adiabatic formulation. *Mon. Wea. Rev.*, **113**, 1910–191.

——, J. Coté, and A. Staniforth, 1983: The accuracy of a finite-element vertical discretization scheme for primitive equation models: Comparison with finite difference scheme. *Mon. Wea. Rev.*, **111**, 2298–2318.

Bourke, W., 1972: An efficient one-level primitive equation spectral model. *Mon. Wea. Rev.*, **100**, 683–689.

Coté, J., M. Béland, and A. Staniforth, 1983: Stability of vertical discretization schemes for semi-implicit primitive equation models: Theory and application. *Mon. Wea. Rev.*, **111**, 1189–1207.

Daley, R., C. Girard, J. Henderson, and I. Simmonds, 1976: Short-term forecasting with a multilevel spectral primitive equation model. Part I: Model formulation. *Atmosphere*, **14**, 98–134.

Edmon, H. J., B. J. Hoskins, and M. E. McIntyre, 1980: Eliassen-Palm cross sections for the troposphere. *J. Atmos. Sci.*, **37**, 2600–2616.

Eliasen, E. B., B. Machenhauer, and E. Rasmussen, 1970: On a numerical method for integration of the hydrodynamical equations with a spectral representation of the horizontal fields. Rep. No. 2, Institute of Theoretical Meteorology, Copenhagan University, Copenhagan, 35 pp.

Hartmann, D. L., 1988: On the comparison of finite-element to finite-difference methods for the representation of vertical structure in model atmospheres. *Mon. Wea. Rev.*, **116**, 269–273.

Karoly, D. J., 1990: The role of transient eddies in low-frequency zonal variations in the Southern Hemisphere circulation. *Tellus*, **42A**, 41–50.

Kidson, J. W., 1988: Indices of the Southern Hemisphere zonal wind. *J. Climate,* **1,** 183–194.

Lorenz, E. N., 1951: Seasonal and irregular variations of the Northern Hemisphere sea level pressure profile. *J. Meteor.,* **8,** 52–59.

Manabe, S., J. Smagorinsky, and R. F. Strickler, 1965: Simulated climatology of a general circulation model with a hydrologic cycle. *Mon. Wea. Rev.,* **93,** 769–798.

Namias, J., 1950: The index cycle and its role in the general circulation. *J. Meteor.,* **7,** 130–139.

Nigam, S., 1990: On the structure of variability of the observed tropospheric and stratospheric zonal-mean zonal wind. *J. Atmos. Sci.,* **47,** 1799–1813.

Phillips, N. A., 1957: A coordinate system having some special advantages for numerical forecasting. *J. Meteor.,* **14,** 184–185.

Randel, W. J., 1990: Coherent wave–zonal mean flow interactions in the troposphere. *J. Atmos. Sci.,* **47,** 439–456.

Robert, A. J., J. Henderson, and C. Turnbull, 1972: An implicit time integration scheme for baroclinic models of the atmosphere. *Mon. Wea. Rev.,* **100,** 329–335.

Robinson, W. A., 1991: The dynamics of the zonal index in a simple model of the atmosphere. *Tellus,* **43A,** 295–305.

Rossby, C.-G., 1939: Relations between variations in the intensity of the zonal circulation and the displacements of the semi-permanent centers of action. *J. Mar. Res.,* **2,** 38–55.

Simmons, A. J., and B. J. Hoskins, 1977: Baroclinic instability on the sphere: Normal modes of the primitive and quasi-geostrophic equations. *J. Atmos. Sci.,* **34,** 581–588.

——, and ——, 1978: The life-cycles of some nonlinear baroclinic waves. *J. Atmos. Sci.,* **35,** 414–432.

Trenberth, K. E., 1979: Interannual variability of the 500-mb zonal mean flow in the Southern Hemisphere. *Mon. Wea. Rev.,* **107,** 1515–1524.

——, 1984: Interannual variability of the Southern Hemisphere circulation; Representativeness of the year of the global Weather Experiment. *Mon. Wea. Rev.,* **112,** 108–125.

Webster, P. J., and J. L. Keller, 1975: Atmospheric variations: Vacillations and index cycles. *J. Atmos. Sci.,* **32,** 1283–1300.

Willett, H. C., 1948: Patterns of world weather changes. *Trans. Amer. Geophys. Union,* **29,** 803–809.